Surface Science 623 (2014) 17–24

Contents lists available at ScienceDirect

Surface Science

journal homepage: www.elsevier.com/locate/susc

Two-dimensional bismuth–silver structures on Si(111)

N.V. Denisov [a,b], E.N. Chukurov [a], Yu.V. Luniakov [a,b], O.A. Utas [a,b], S.G. Azatyan [a,b], A.A. Yakovlev [a], A.V. Zotov [a,b,c], A.A. Saranin [a,b,*]

[a] Institute of Automation and Control Processes FEB RAS, 5 Radio Street, 690041 Vladivostok, Russia
[b] School of Natural Sciences, Far Eastern Federal University, 690950 Vladivostok, Russia
[c] Department of Electronics, Vladivostok State University of Economics and Service, 690600 Vladivostok, Russia

ARTICLE INFO

Article history:
Received 28 October 2013
Accepted 6 January 2014
Available online 15 January 2014

Keywords:
Atom-solid interactions
Silicon
Bismuth
Silver
Scanning tunneling microscopy
DFT calculations

ABSTRACT

Using scanning tunneling microscopy (STM) observations, it has been found that deposition of 0.8–1.3 monolayer of Ag onto the mixed Si(111)$\alpha-\sqrt{3}\times\sqrt{3}$ / $\beta-\sqrt{3}\times\sqrt{3}$-Bi surfaces followed by annealing at 150–250°C induces formation of new ordered and quasi-ordered (Bi,Ag)/Si(111) metastable structures, $\sqrt{19}\times\sqrt{19}$, 4×4, $2\sqrt{3}\times2\sqrt{3}$, and '$3\sqrt{3}\times3\sqrt{3}$'. Scanning tunneling spectroscopy has demonstrated that the $2\sqrt{3}\times2\sqrt{3}$ structure is semiconducting, while the $\sqrt{19}\times\sqrt{19}$ and 4×4 structures are metallic. Structural models of the $\sqrt{19}\times\sqrt{19}$ and 4×4 have been proposed based on placing a single Ag(111)1×1 layer with selected Ag atoms being substituted for Bi atoms onto the bulk-like Si(111)1×1 surface. The models have been proved with DFT calculations and comparison of simulated and experimental STM images. Calculated band structure of the Si(111)4×4 structure displays a spin–split metallic surface-state band with splitting of $\Delta k \approx 0.002$ Å^{-1} and $\Delta E \approx 10$ meV in the vicinity of the Fermi level.

1. Introduction

To design future spintronic devices, materials with controlled spin-polarization, capability to transport spin-polarized current and ability to work being an ultra-thin film or a nanoparticle are strongly demanded. The promising materials possessing such properties are surface reconstructions or surface alloys with the Rashba effect. Vivid examples of Rashba-effect materials are the Si(111)$\beta-\sqrt{3}\times\sqrt{3}$-Bi surface reconstruction and $BiAg_2$ surface alloy (Ag(111)$\sqrt{3}\times\sqrt{3}$-Bi structure) which demonstrate a giant spin–orbit splitting of surface-state bands [1–9]. However, the Si(111)$\beta-\sqrt{3}\times\sqrt{3}$-Bi structure is semiconducting and its spin–orbit splitting is located in the valence zone without crossing the Fermi level [1–3]. This means that it does not allow significant spin transport. In contrast, the other structure ($BiAg_2$) is a metallic surface structure which has an amazing giant spin–orbit splitting of its bands below and above the Fermi level [4,5,7–9]. However, the main drawback of this structure is that the substrate under the surface alloy is also metallic, while the substrate is preferred to be a semiconductor for using in spintronics. It is also desired that a new spintronic structure can be easily combined with current or perspective Si surface technologies. That is, the substrate should preferably be silicon.

Thus, the main goal of our investigation was to form an ultra-thin bismuth–silver structure directly on Si(111). We have found four new one-atomic-layer bismuth–silver structures, including the well-ordered 4×4 and $2\sqrt{3}\times2\sqrt{3}$, poorly-ordered $\sqrt{19}\times\sqrt{19}$, and quasi-ordered '$3\sqrt{3}\times3\sqrt{3}$'. Among them, the metallic 4×4 structure has been concluded to be an Ag(111) layer where several Ag atoms are substituted for Bi atoms. DFT calculations have confirmed that its band structure contains spin–split metallic surface-state band.

2. Experimental and calculation details

The experiments were carried out with Omicron STM operated in an ultrahigh vacuum (~7.0×10^{-11} Torr). Atomically-clean Si(111)7×7 surfaces were prepared in situ by flashing to 1280 °C after the samples were first outgassed at ~600 °C for several hours. Ag and Bi were deposited from commercial cells HTEZ40. Deposition rate of Ag was calibrated by formation of the Si(111)$\sqrt{3}\times\sqrt{3}$-Ag surface containing 1 monolayer of Ag [10]. (1 monolayer (ML) = 7.83×10^{14} atoms/cm^2 for Si(111).) Deposition rate of Bi was calibrated using Si(111)$\beta-\sqrt{3}\times\sqrt{3}$-Bi surface (1 ML Bi [11]) as a reference by room temperature (RT) deposition of Bi onto Si(111)7×7 followed by annealing at 470–500°C. Additional checking of the Bi deposition rate was done with Si(111)$\alpha-\sqrt{3}\times\sqrt{3}$-Bi (1/3 ML Bi [11], prepared by Bi desorption from the $\beta-\sqrt{3}\times\sqrt{3}$-Bi) to which Bi was deposited at RT followed by 270 °C heating to convert it to the $\beta-\sqrt{3}\times\sqrt{3}$-Bi structure. The checking proved that there is no apparent Bi desorption at 470–500°C. The details of the mixed $\alpha-\sqrt{3}\times\sqrt{3}$ / $\beta-\sqrt{3}\times\sqrt{3}$-Bi surface preparation are given in Section 3. Annealing temperature of the samples in the range of 100–600°C was measured by thermocouple.

* Corresponding author at: Institute of Automation and Control Processes, 5 Radio Street, 690041 Vladivostok, Russia. Fax: +7 4232310452.
E-mail address: saranin@iacp.dvo.ru (A.A. Saranin).

0039-6028/$ – see front matter © 2014 Elsevier B.V. All rights reserved.
http://dx.doi.org/10.1016/j.susc.2014.01.003

Structural models of the (Bi,Ag)/Si(111) surface structures were calculated using the plane-waves total-energy calculations based on density functional theory (DFT) [12] with projector-augmented wave pseudopotentials [13] using Vienna Ab Initio Simulation Package (VASP) [14,15]. For the exchange and correlation functional, the generalized gradient approximation (GGA) [16] has been employed. The electronic wave functions were expanded in a plane-wave basis set with an energy cutoff of 20 Ry. The surface was simulated by periodic slab geometry with a calculated structure unit supercell containing eight Si atomic layers and Bi–Ag layer according to the proposed model. The dangling bonds of the bottom slab layer were saturated by hydrogen atoms, which as well as bottom bilayer silicon atoms were fixed, while the rest atoms were free to move. A vacuum region of approximately 15 Å was incorporated within each periodic unit cell to prevent interaction between adjacent surfaces. The geometry was optimized until the total energy is converged to 10^{-4} eV and the total force is converged to 10^{-3} eV/Å. The sensitivity of formation energies on kinetic energy cutoff, k-points setup, and the total energy/force numerical accuracy has been tested and found to have a negligible effect on the total energy differences. The Hamiltonian contains the scalar relativistic correlations, and the spin–orbit interaction was taken into account by the second variation method as has been implemented in VASP [17]. Simulated STM images of the relaxed models were generated from local density of states (DOS) according to Tersoff–Hamann approach [18].

3. Results and discussion

In the beginning it is worth noting that coadsorption of Ag and Bi onto Si(111) surface does not always lead to the formation of the new (Bi,Ag)/Si(111) surface structures. Say, RT codeposition of Bi and Ag onto Si(111)7 × 7 followed by annealing results in the surface which contains domains of √3 × √3-Ag and β − √3 × √3-Bi (for Ag coverage less than 1 ML) or the √3 × √3-Ag surface with Bi islands (for larger Ag coverage). The former surface (mixture of √3 × √3-Ag and β − √3 ×√3-Bi domains) develops also when Bi is deposited onto the Ag/Si(111) surface which comprises the mixture of √3 × √3-Ag and 6 × 1-Ag phases, while the latter surface (√3 × √3-Ag with Bi islands) develops when Bi is deposited onto the √3 × √3-Ag surface followed by annealing. Note that this is contrasted to (Sn,Ag)/Si(111) system, where the new Si(111)2 × 2-(Sn,Ag) structure appears after RT Sn deposition onto the √3 × √3-Ag followed by annealing [19].

Thus, Si(111)7 × 7 and Ag/Si(111) surfaces did not prove to be suitable templates for growing 2D (Bi,Ag) alloys on Si(111) and we paid the main attention to the Bi/Si(111) surfaces. Remind that Bi induces two one-atomic-layer structures on the bulk-like Si(111) surface, α − √3 × √3-Bi and β − √3 × √3-Bi with 1/3 and 1 ML Bi, respectively [11]. The β − √3 × √3-Bi can be formed directly by RT deposition of 1 ML Bi onto Si(111)7 × 7 surface followed by annealing. The α − √3 × √3-Bi can be prepared only by Bi desorption from the β − √3 × √3-Bi. The main defects of the α − √3 × √3-Bi structure are substitutional Si atoms, which substitute, according to our STM observations, up to ~10–12% (~0.033–0.04 ML) of Bi atoms. The β − √3 × √3-Bi is free of such defects.

Deposition and annealing of Ag on the "monopolistic" β − √3 × √3-Bi surface results in formation of the high Ag islands with flat tops, i.e. again no 2D (Bi,Ag) alloys develop. However, when Ag is deposited onto the "monopolistic" α − √3 × √3-Bi surface at RT (as well as after following annealing at ~250 °C), a maze-like structure forms (Fig. 1a), where Ag atoms take adsorption sites without destroying the underlying α − √3 × √3-Bi structure. This maze structure accumulates about 1.0 ML Ag weakly bonded to the surface, hence it appears to be sensitive to the electric field of the STM tip. As an example, Fig. 1 shows a set of STM images acquired successively from the same surface area. Empty-state image (Fig. 1a) shows the surface completely covered by the maze structure. However, when the bias polarity is changed and filled-state image is acquired (Fig. 1b), the most of Ag layer is removed baring the underlying α − √3 × √3-Bi surface. The left fragments of the maze structure are believed to be anchored to the substitutional Si defects. Assumption is based on the observation that the Si-defect density at the denuded regions is noticeably less than that at the original the α − √3 × √3-Bi surface (~3% versus ~12%). This could be accounted to the fact that while Bi atoms in α − √3 × √3-Bi structure have lone electron pairs (hence, are chemically inert) while substitutional Si atoms have unsaturated dangling bonds (hence, are chemically active). When the bias polarity is changed back and empty-state images are acquired, the maze structure gradually recovers (Fig. 1c and d). Thus, the maze structure can be thought as an Ag adlayer on α − √3 × √3-Bi surface. Note that adatom manipulation by tip-generated electric field is a well-known phenomenon. Its mechanism was understood in terms of interaction of dipole associated with adsorbate atom and nonuniform electric field under the STM tip [20,21]. Depending on the tip bias polarity, the static dipole is either attracted towards the region of the maximum field strength (i.e., underneath the tip apex) or repelled away from it. The vivid examples were given by STM-induced manipulations of In on Si(111) [22] or Tl on Si(100) [23]. In the present study, removal of Ag atoms with positive tip bias and their recovery with negative tip bias imply that the negative charge is transferred from adsorbed Ag atom to the substrate.

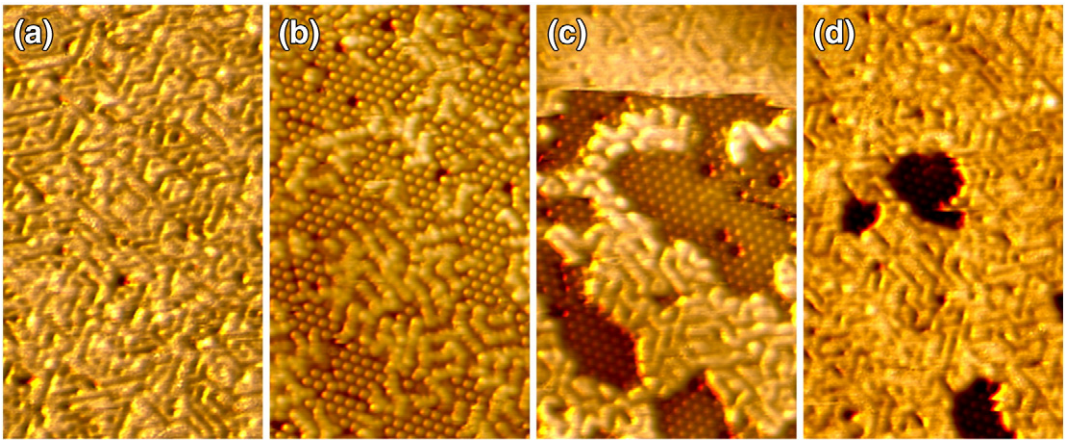

Fig. 1. Sequence of 150 × 250 Å^2 STM images of the maze structure successively recorded from the same area with changing the sample bias voltage. (a) Empty-state image ($V_s = +1.5$ V) of the initial maze structure. (b) Successive filled-state image ($V_s = -1.5$ V). (c) and (d) Successive empty-state images ($V_s = +1.5$ V) recorded after (b).

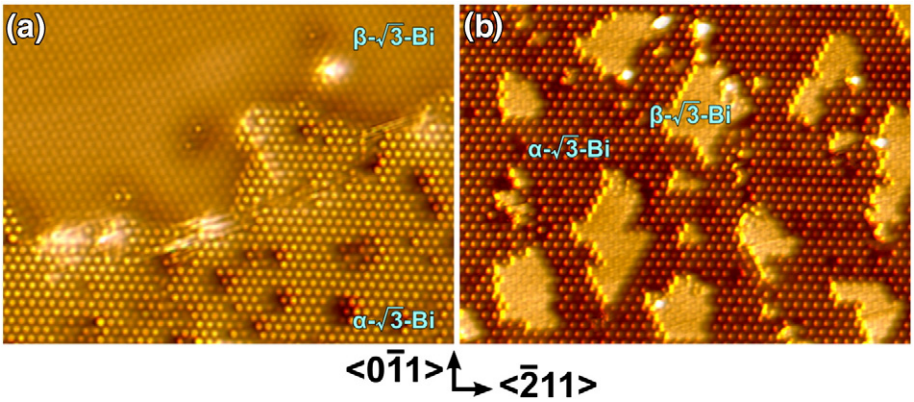

Fig. 2. 300 × 225 Å^2 filled-state STM images ((a) ($V_s = -1$V) and (b) ($V_s = -2$V)) of the initial mixed α-√3 × √3/β-√3 × √3-Bi Si(111) surface prepared under different conditions (see the text).

It appears that the only way to form the 2D (Bi,Ag) alloys on Si(111) is to use the initial surfaces which resemble a mixture of the α − √3 × √3-Bi and β − √3 × √3-Bi structures. Since the resultant (Bi,Ag)/Si(111) surface structure was found to depend on the area fractions occupied by α − √3 × √3 and β − √3 × √3-Bi (hereafter, we will operate with the area fraction occupied by β − √3 × √3-Bi, F_β), as well as size and surface distribution of their domains, we paid especial attention to the surface preparation procedure. The mixed α − √3 × √3 / β − √3 × √3 surface can be prepared in two ways. The first one is to deposit of 0.8–1.2 ML Bi (depending on the desired fraction of β − √3 ×√3-Bi) at RT onto Si(111)7 × 7 and to anneal it at ~600–650°C. The main weakness of this method is the non-uniform distribution of the β − √3 × √3-Bi over the surface (Fig. 2a): the β − √3 × √3-Bi domains are large and are often extended along one of the directions. The second way is preferable to get small β − √3 × √3-Bi domains uniformly distributed over the surface (Fig. 2b). First, the α − √3 × √3-Bi structure is formed over the entire surface (~0.65 ML Bi deposition at RT onto the 7 × 7, followed by a 600 °C annealing). Then, additional Bi is deposited at RT to obtain required F_β (0.01 ML Bi for ~1.5% of the β − √3 × √3-Bi surface fraction) and annealed at ~270 °C. The side effect of this method is the formation of small random Si islands seen as extra bright protrusions near edges of the β − √3 × √3-Bi domains (Fig. 2b). They are plausibly originated from the substitutional Si atoms of the initial α − √3 × √3-Bi area during its transformation to the β − √3 × √3-Bi. Upon subsequent (Bi,Ag)/Si(111) growth, these Si atoms can induce formation of small patches of the √3 × √3-Ag structure, which is known to adopt 1.0 ML Si [24].

If the initial surface has small areas of the β − √3 × √3-Bi structure with the total surface fraction less than 10%, then deposition of ~1 ML Ag followed by ~250 °C annealing results in the formation of the new √19 × √19 − $R \pm 23.4°$ (Bi,Ag)/Si(111) structure (Fig. 3a, b) which occupies up to ~75% of the surface area (at F_β ~10%). Depending on the

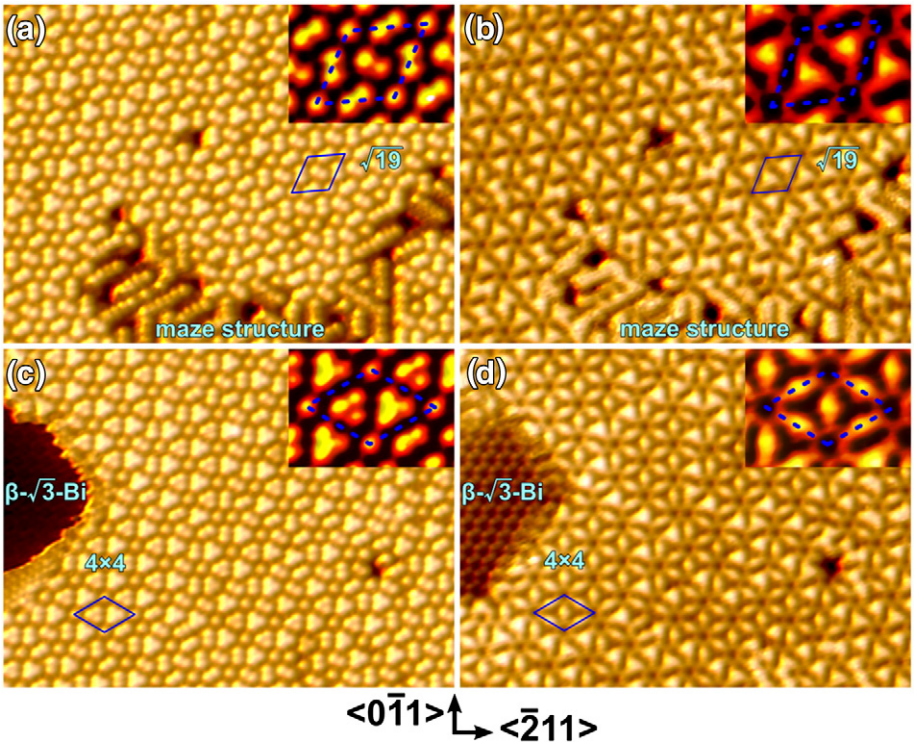

Fig. 3. 200 × 150 Å^2 filled-state ($V_s = -1.5$ V) and empty-state ($V_s = +1.5$ V) STM images for the √19 × √19 (a, b) and 4 × 4 (c, d) structures, respectively. The maze structure stabilized by another (Bi,Ag) structure is also present in (a) and (b). The 4 × 4 STM images (c, d) are selected to demonstrate the √19 × √19 to 4 × 4 structure transition (see the text). Unit cells of the √19 × √19 and the 4 × 4 are outlined. Insets present enlarged STM images with enhanced contrast showing single unit cell for each of the structures. The main crystallographic directions are shown.

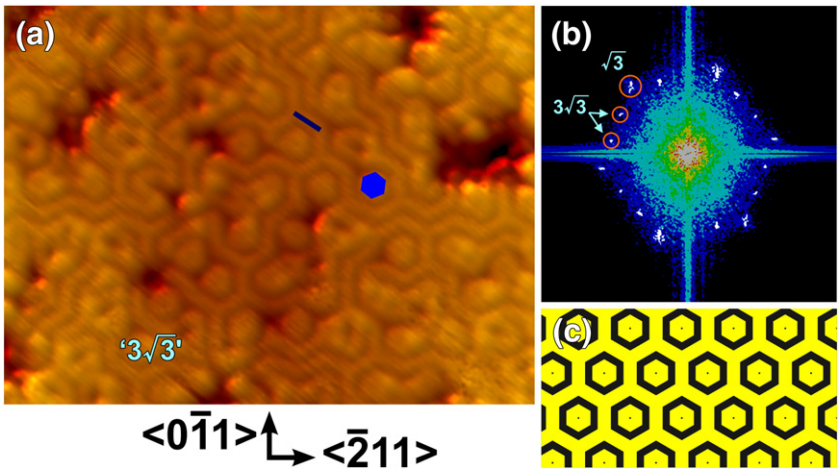

Fig. 4. (a) 200 × 150 Å^2 empty-state ($V_s = +1.5$ V) STM image of the quasi-3√3 × 3√3-(Bi,Ag)/Si(111) structure. Blue objects demonstrate main elements of the structure, stick and hexagon. (b) FFT pattern from the surface with coexisting α-√3 × √3-Bi and quasi-3√3 × 3√3-(Bi,Ag) structures. The √3 and 3√3 reflections are indicated. (c) Schematic presentation of an ideal well-ordered array of the 3√3 × 3√3-(Bi,Ag) structure.

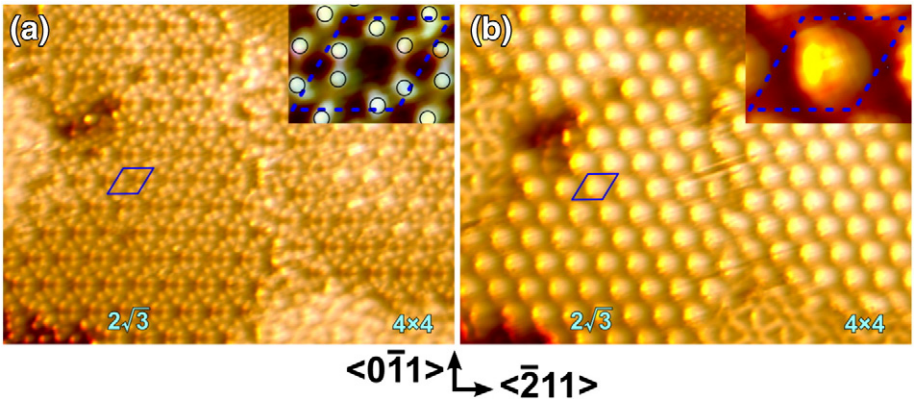

Fig. 5. 200 × 150 Å^2 filled-state ($V_s = -1.5$ V) (a) and empty-state ($V_s = +1.5$ V) (b) STM images of the 2√3 × 2√3-(Bi,Ag) structure. Enhanced-contrast STM images of a single 2√3 × 2√3 unit cell are shown in the insets. The 2√3 × 2√3 unit cell is outlined.

bias polarity, the structure has a very different STM appearance. Filled-state STM image of the √19 × √19 displays seven bright protrusions per the unit cell (Fig. 3a, inset): one single protrusion placed in a cell corner (T_1 site); the other are grouped in two large triangles. The triangles are centered over H_3 and T_4 positions and rotated (clockwise for R-23.4° domain, counterclockwise for R + 23.4° domain) relative to the triangle of half unit cell, so that each protrusion of the triangle is located near edge of the half cell. Closest protrusions of the two neighbor unit cells create a pair. The length of this pair is about 5 Å, which is close to the length of √3 period on the Ag(111)1 × 1 surface. In the empty-state STM image (Fig. 3b, inset), one can see the depressions located in the positions where the protrusions in the filled-state image are located. The unit cell contains also two bright distorted triangles rotated relative to each other.

The √19 × √19 array is poorly ordered since it tends to transform into the other more stable (Bi,Ag)/Si(111) structure, namely 4 × 4 (Fig. 3c, d). The 4 × 4 starts to appear when F_β exceeds 10%, in which case the 4 × 4 and √19 × √19 form combined arrays where one of the structures smoothly changes to another, as one can see in Fig. 3c and d. Usually, the edge where the √19 × √19 prevails is bounded to the α − √3 × √3-Bi region, while the 4 × 4 neighboring structure is the β − √3 × √3-Bi. This means that the √19 × √19 is formed due to Bi deficit in a local area. According to our consideration (to be shown later when presenting structural models), the 4 × 4 is expected to occupy

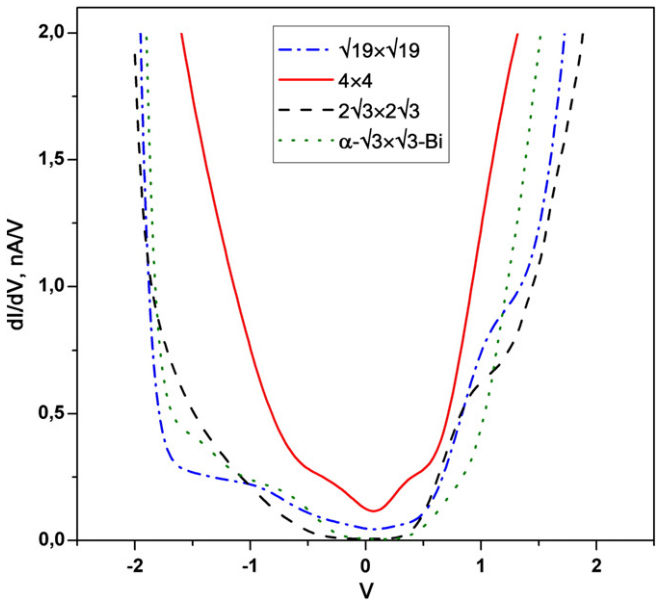

Fig. 6. Spectra of conductivity of the √19 × √19, 4 × 4, 2√3 × 2√3 (Bi,Ag)/Si(111) structures, and that of the α-√3 × √3-Bi given for comparison.

maximal surface fraction at $F_\beta \approx 20\%$. In reality, however, certain amount of Ag atoms agglomerates into 3D Ag islands and does not participate in the (Bi,Ag)/Si(111) structure formation. Maximal 4×4 surface fraction (~80%) is obtained at $F_\beta \approx 35\%$, deposition of ~1 ML Ag and annealing at ~250 °C. Filled-state STM images of the 4×4 structure display seven bright protrusions per 4×4 unit cell (Fig. 3c, inset): a single one located in the cell corner (T_1 site) and the other six grouped in two triangles, one triangle being brighter than the other. The length of a side of the 4×4 triangle is approximately equal the $\sqrt{3}$ period of the Ag(111)1×1 surface (~5 Å). The triangles are plausibly located over H_3 and T_4 sites. Empty-state STM images show depressions in positions of filled-state protrusions with single hollows coupled by bright rods (Fig. 3d, inset).

When a surface with $F_\beta \approx$ 10–20% is covered by ~0.8 ML Ag and annealed at ~150 °C, about 80% of the surface becomes occupied by the new (Bi,Ag)/Si(111) structure. Its long-range order is not apparent in STM images (Fig. 4a), but the fast Fourier analysis reveals occurrence of the $3\sqrt{3} \times 3\sqrt{3}$ periodicity (Fig. 4b). Thus, we define this structure

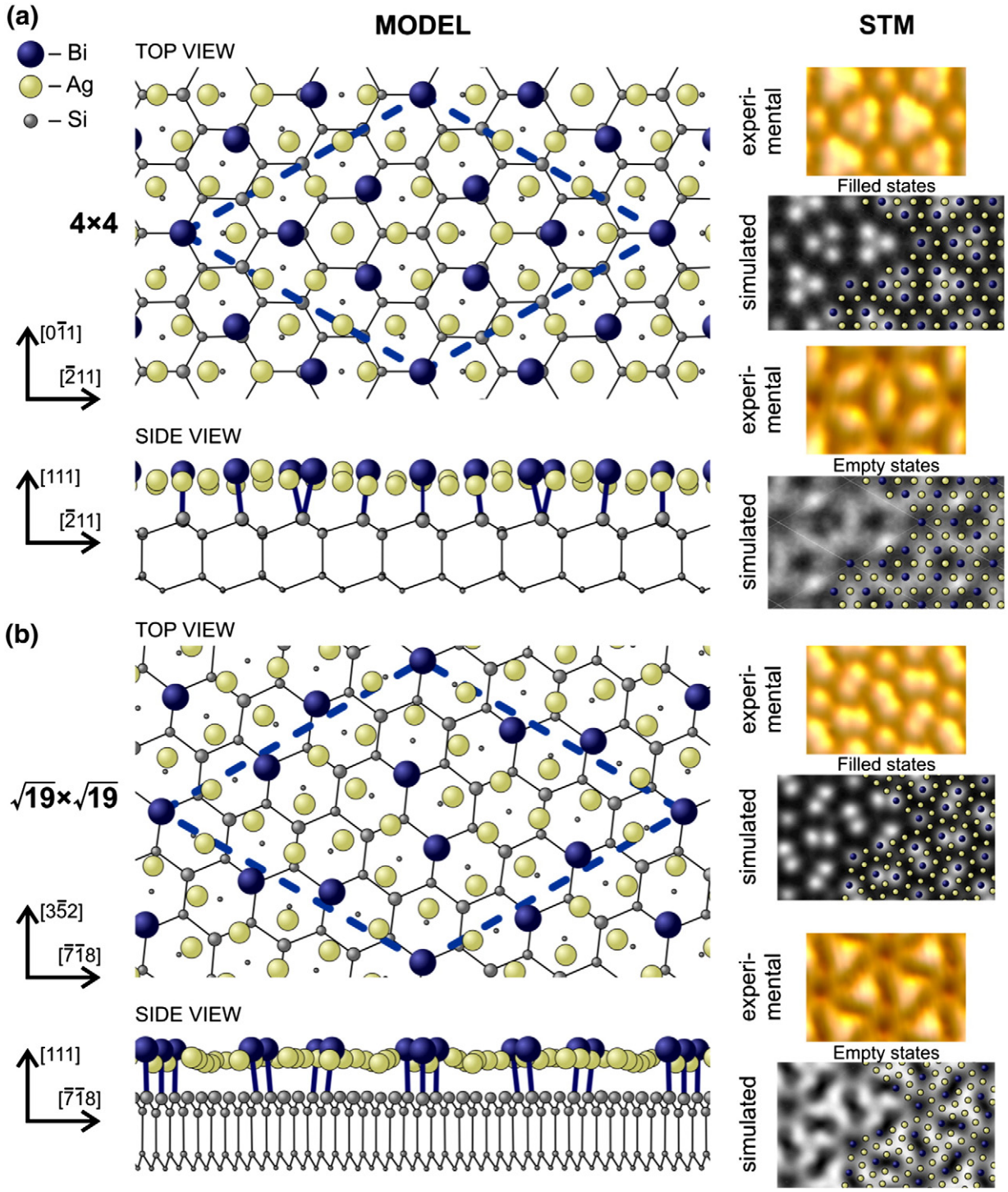

Fig. 7. Atomic models of the 4×4 (a) and $\sqrt{19} \times \sqrt{19}$ (b) (Bi,Ag)/Si(111) structures with corresponding experimental and simulated STM images. The scale of the models is the same for the both structures. The corresponding unit cells are outlined. The size of the balls, indicating atoms, reduces with increasing distance from the top for the both top and side views. Dark blue lines indicate the bonds between Bi and the closest underlying Si atoms. The scale of the experimental and simulated STM images is the same and specific for each individual structure. The simulated images are superposed with Bi–Ag layer of the corresponding model.

quasi-3√3 × 3√3 (or '3√3 × 3√3'). STM images show that the structure is built of two basic elements. The first one is a bright stick (marked as blue bar in Fig. 4a), three Si(111)1 × 1 unit lengths long, which can be linked with one or two other same sticks. The angle between two linked sticks equals 120°. If only these sticks form a structure, then the structure would be an array of large honeycombs with 3√3 × 3√3 periodicity. The second element is a small honeycomb (marked as blue small hexagon in Fig. 4a) with the side of ~5 Å (close to √3 of the Ag(111) unit length). The close-packed array of these small honeycombs would have a √13 × √13 periodicity. The real quasi-3√3 × 3√3-(Bi, Ag) structure is a mixture of these base elements, but the ideal structure must be an array of the conjugate large honeycombs, each of them has the small honeycomb placed in its center as shown in Fig. 4c. Nonetheless, even a single completed unit cell cannot be found in STM images. The '3√3 × 3√3' can also exist on the surface after annealing at higher temperature, but it occupies much smaller area fraction.

One more (Bi,Ag)/Si(111) structure, 2√3 × 2√3, (Fig. 5) is formed occupying up to ~75% surface area when ~0.8–1.0 ML Ag is deposited onto the surface with $F_\beta \approx$ 15–20% and annealed at ~250 °C. The 2√3 × 2√3 unit cell in the filled-state STM image displays six protrusions (Fig. 5a, inset), which can often have slightly elongated shape and variable brightness. The brightest protrusions (marked in the inset in Fig. 5a by black circles) form an irregular hexagon with two different alternating sides ~4 and ~5.5 Å long. Empty-state STM image of the 2√3 × 2√3 demonstrates one large protrusion having the shape of a convex triangle (Fig. 5b, inset). If one combines the filled-state and empty-state images then the irregular hexagon frames the convex triangle with the common center in T_1. Each vertex of the convex triangle is always pointed to large side of the irregular hexagon and directed towards the $\langle \bar{2}11 \rangle$ crystallographic direction.

Deposition of Ag onto the new (Bi,Ag)/Si(111) structures followed by annealing results mainly in formation of 3D Ag islands placed far from each other, indicating high mobility of Ag adatoms on these surface structures. Additional RT Bi deposition onto the (Bi,Ag)/Si(111) structures followed by annealing leads to appearance of the β-√3 × √3-Bi or increasing of its area fraction, decreasing of the fractions of the (Bi,Ag) structures and, often, appearance of 3D Ag islands.

Annealing of the (Bi,Ag)/Si(111) structures at 300 °C or above results in beginning of the √3 × √3-Ag formation (with splitting of the surface in two levels because the √3 × √3-Ag adopts 1.0 ML Si [24]), changing the (Bi,Ag)/Si(111) structures' surface fraction and complete disappearance of the α − √3 × √3-Bi (if it was on the surface before the heating). The 400 °C annealing destroys all the new structures and only the √3 ×√3-Ag and β-√3 × √3-Bi domains (if the total Ag coverage is less than 1 ML) are left on the surface.

Fig. 6 presents spectra of scanning tunneling spectroscopy (STS) of the (Bi,Ag)/Si(111) structures, √19 × √19, 4 × 4, 2√3 × 2√3, and that of the α − √3 × √3-Bi given for comparison. STS study of the maze structure was not carried out because of its sensitivity to the tip electric field. The quasi-3√3 × 3√3 was not considered, since its structure does not display apparent long-range ordering. One can see that the 4 × 4 and √19 × √19 are metallic, while the 2√3 × 2√3 as well as the α − √3 × √3-Bi are semiconductors. The metallic nature of the 4 × 4 is more pronounced than that of the √19 × √19. Therefore, the 4 × 4 is believed to be the most promising candidate as a two-dimensional metallic material with a spin–orbit splitting effect, provided that its properties are akin the $BiAg_2$ surface alloy.

Promising metallic properties of the √19 × √19 and 4 × 4 stimulated us to construct models of these structures. Modeling was based on the following assumptions. First, filled-state STM images are supposed to show protrusions from Bi atoms, while empty-state images reveal Ag–Ag bonds (by analogy with (Sn,Ag) surface alloy on Si(111) [19]). Second, the structures are supposed to incorporate basically a single Ag(111)1 × 1 layer atop the bulk-like Si(111) surface. This is based on the total coverage of Ag and Bi (which is close to the coverage of the Ag(111) single layer, 1.77 ML) and zero Si coverage (absence of noticeable Si mass transport during (Bi,Ag)/Si(111) structure formation indicates that the structures have the same Si coverage as the α − √3 × √3 and β − √3 × √3-Bi, 0 ML). Thus, the initial models were as follows: a single Ag(111)1 × 1 layer rotated by 30° for the 4 × 4 and ± ~27.6° for the √19 × √19, respectively, and stretched by ~2.3% and ~4.1%, respectively, is placed on the bulk-like Si(111) surface in such a way that zero-point Ag atom takes T_1 site. Seven Bi atoms per unit cell substitute Ag atoms: the solitary Bi atoms (in the corner of the unit cells) take T_1 sites, while the other six Bi atoms reside near T_4 sites according to the location protrusions in the filled-state STM images. First-principles DFT calculations of these models show the verity of our suppositions. The relaxed models of the 4 × 4 and √19 × √19 structures on the Si(111) surface as well as their experimental and simulated STM images are presented in Fig. 7a and b. One can see that model-based simulated STM images reproduce nicely all the features seen in the experimental images. Compositions adopted in the models are consistent with those evaluated in the experiment (see Table 1). It is worth to remark that the average distance between levels of Bi and Ag atoms of ~0.58 Å (the range 0.37–0.78 Å) for the √19 × √19 and ~0.59 Å (0.37–0.79 Å) for the 4 × 4 are close to the distance between Bi atoms' level and Ag atoms' level of the Ag(111)√3 × √3-Bi surface alloy, which is 0.57 Å (experimental) or 0.61 Å (calculated) [25].

Since all the above consideration implies the 4 × 4 structure to be the most promising candidate for observing large spin splitting of metallic surface-state bands, we have calculated its electron band structure and density of states. The results of calculations are presented in Fig. 8. As expected, the band structure of the 4 × 4 contains several spin-split bands one of which is metallic crossing the Fermi level between $\bar{\Gamma}$ and $\bar{K}$ points (Fig. 8a, b). However, it should be admitted that this band is shallow (less than 100 meV below the Fermi level) and its splitting near the Fermi level is rather modest, momentum splitting $\Delta k \approx 0.002$ Å^{-1} and energy splitting $\Delta E \approx 10$ meV. These values are an order of magnitude lower than those achieved recently in spin-split metallic bands on semiconductor surfaces in other material systems. For example, for the Ge(111)√3 × √3 − Pb $\Delta k \approx 0.04$ Å^{-1} and $\Delta E \approx 200$ meV [26], for the Ge(111)√3 × √3-Au $\Delta k \approx 0.04$ Å^{-1} [27], and for the Tl-modified Si(111)√3 × √3-Au $\Delta k \approx 0.05$ Å^{-1} and $\Delta E \approx 190$ meV [28]. As for the calculated DOS spectrum of the 4 × 4 structure (Fig. 8c), it demonstrates occurrence of three peaks in the range from −0.6 to 0 eV (−0.52, −0.22, and −0.04 eV), as well as the +0.54 eV peak above

Table 1
Experimental and model compositions of the (Bi,Ag) structures and main conditions for their formation.

(Bi,Ag)/Si(111) structure	Experimental		Model				Main condition
	Bi, ML	Ag, ML	Bi		Ag		
			ML	atoms	ML	atoms	
Maze	~0.3	~1–1.1					$F_\beta = 0$ %, T = [RT, 250 °C]
√19 × √19	~0.35	~1.2	~0.37	7	~1.26	24	$F_\beta \approx 10$%, T = 250 °C
4 × 4	~0.4	~1.2	~0.44	7	1.25	20	$F_\beta \approx 20$%, T = 250 °C
'3√3 × 3√3'	~0.4	~0.8					$F_\beta > 0$%, T = 150 °C
2√3 × 2√3	~0.5	~1.2					$F_\beta \approx 30$%, T = 250 °C

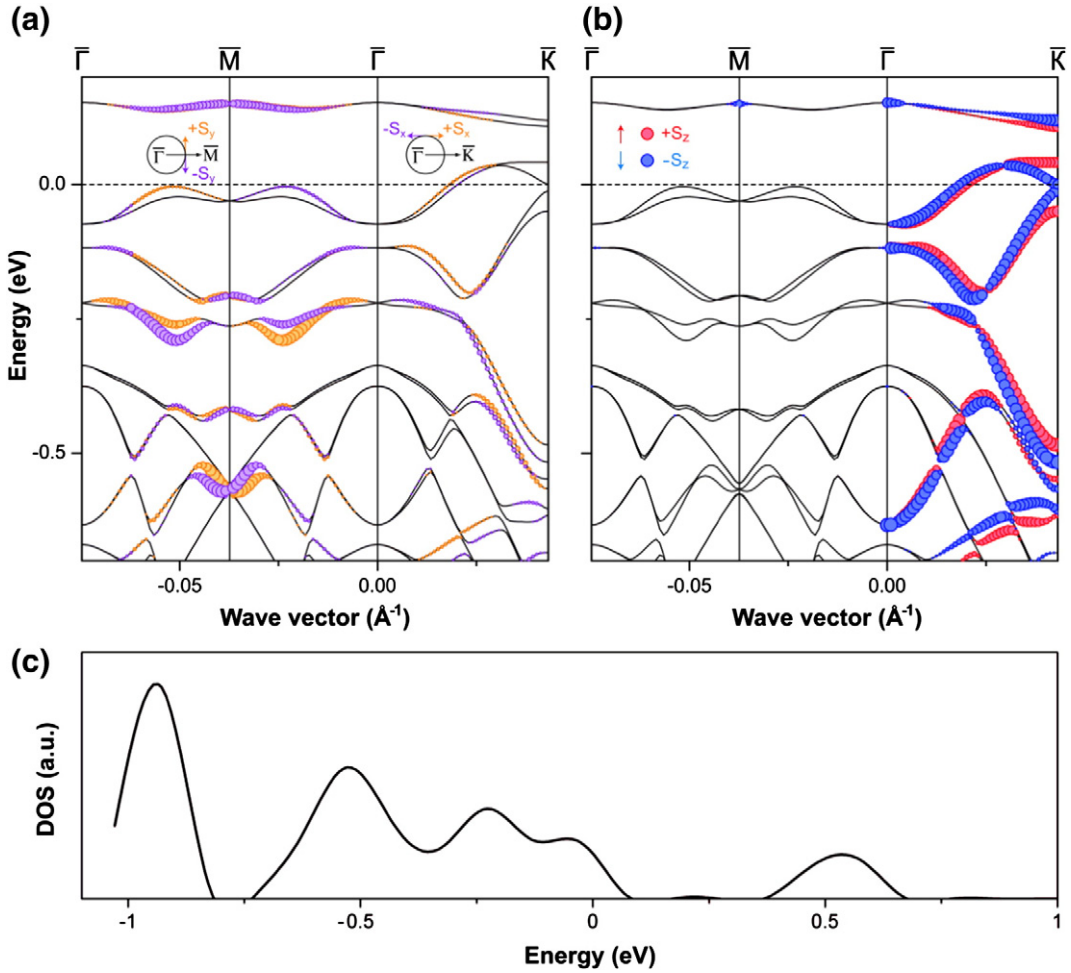

Fig. 8. Energy-band dispersions including spin–orbit coupling illustrating the in-plane (a) and out-of-plane (b) spin polarization components and total DOS (c) for the 4×4 reconstruction. The diameter of the circles in (a) and (b) is proportional to the spin polarization and to contributions of the Ag and Bi atoms at the surface layer. Different colors represent opposite spin polarizations according to the schemes. S_x and S_y spin components are nearly zero at Γ–M and Γ–K directions, respectively.

the Fermi level. These features show up as shoulders in the experimental STS spectrum of the 4×4 (Fig. 6) demonstrating a reasonable agreement between the band calculations and experimental STS data.

4. Conclusions

Using STM observations, several new (Bi,Ag) one-atomic-layer structures on Si(111) surface have been found. Except for the so-called maze structure which forms on the "monopolistic" $\alpha - \sqrt{3} \times \sqrt{3}$-Bi surface as a partially ordered Ag atomic adlayer, the other four structures, $\sqrt{19} \times \sqrt{19}$, 4×4, quasi-$3\sqrt{3} \times 3\sqrt{3}$, and $2\sqrt{3} \times 2\sqrt{3}$, develop only on the mixed $\alpha - \sqrt{3} \times \sqrt{3}$ / $\beta - \sqrt{3} \times \sqrt{3}$-Bi surfaces and show up as (Bi,Ag) 2D alloys. Though several structures often coexist on the surface, one of the structures can prevail upon appropriate growth conditions, initial Bi coverage, deposited Ag amount, and annealing temperature (as shown in Table 1). Structural perfection of (Bi,Ag)/Si(111) structures varies from well-ordered 4×4 and $2\sqrt{3} \times 2\sqrt{3}$ through poorly-ordered $\sqrt{19} \times \sqrt{19}$ to quasi-ordered '$3\sqrt{3} \times 3\sqrt{3}$'. STS analysis reveals that while the $2\sqrt{3} \times 2\sqrt{3}$ is semiconducting, the 4×4 and $\sqrt{19} \times \sqrt{19}$ are metallic. According to the structural analysis based on DFT calculations and comparison of simulated and experimental STM images, the latter two structures are plausibly a single Ag(111)1×1 layer rotated relative to the Si substrate, where seven Bi atoms per the 4×4 or $\sqrt{19} \times \sqrt{19}$ unit cell substitute seven Ag atoms to form a new structure. Having this atomic arrangement, the 4×4 has features akin those of the $BiAg_2$ surface alloy. The calculated band structure of the 4×4 surface demonstrates the presence of the metallic surface-state band with modest spin-splitting near the Fermi level, $\Delta k \approx 0.002$ Å^{-1} and $\Delta E \approx 10$ meV. All these findings reveal the 4×4 structure to be a 2D spin-split metallic layer on a semiconductor surface, which has certain prospects to be used in spintronics.

Acknowledgments

Part of this work was supported by the Russian Foundation for Basic Research (Grant Nos 12-02-00416, 13-02-00837, 13-02-12110, 14-02-31070) and the NSh-167.2014.2.

References

[1] I. Gierz, T. Suzuki, E. Frantzeskakis, S. Pons, S. Ostanin, A. Ernst, J. Henk, M. Grioni, K. Kern, C.R. Ast, Phys. Rev. Lett. 103 (2009) 046803.
[2] K. Sakamoto, H. Kakuta, K. Sugawara, K. Miyamoto, A. Kimura, T. Kuzumaki, N. Ueno, E. Annese, J. Fujii, A. Kodama, T. Shishidou, H. Namatame, M. Taniguchi, T. Sato, T. Takahashi, T. Oguchi, Phys. Rev. Lett. 103 (2009) 156801.
[3] E. Frantzeskakis, S. Pons, M. Grioni, Phys. Rev. B 82 (2010) 085440.
[4] C.R. Ast, J. Henk, A. Ernst, L. Moreschini, M.C. Falub, D. Pacile, P. Bruno, K. Kern, M. Grioni, Phys. Rev. Lett. 98 (2007) 186807.
[5] G. Bihlmayer, S. Blugel, E.V. Chulkov, Phys. Rev. B 75 (2007) 195414.
[6] C.R. Ast, G. Wittich, P. Wahl, R. Vogelgesang, D. Pacilé, M.C. Falub, L. Moreschini, M. Papagno, M. Grioni, K. Kern, Phys. Rev. B 75 (2007) 201401(R).
[7] F. Meier, H. Dil, J. Lobo-Checa, L. Patthey, J. Osterwalder, Phys. Rev. B 77 (2008) 165431.
[8] H. Hirayama, Y. Aoki, C. Kato, Phys. Rev. Lett. 107 (2011) 027204.
[9] A. Crepaldi, S. Pons, E. Frantzeskakis, K. Kern, M. Grioni, Phys. Rev. B 85 (2012) 075411.
[10] S. Hasegawa, H. Daimon, S. Ino, Surf. Sci. 186 (1987) 138.
[11] T. Kuzumaki, T. Shirasawa, S. Mizuno, N. Ueno, H. Tochihara, K. Sakamoto, Surf. Sci. 604 (2010) 1044.

[12] W. Kohn, L.J. Sham, Phys. Rev. 140 (1965) A1133.
[13] G. Kresse, D. Joubert, Phys. Rev. B 59 (1999) 1758.
[14] G. Kresse, J. Hafner, Phys. Rev. B 49 (1994) 14251.
[15] G. Kresse, J. Furthmüller, Phys. Rev. B 54 (1996) 11169.
[16] J.P. Perdew, K. Burke, M. Ernzerhof, Phys. Rev. Lett. 77 (1996) 3865.
[17] D. Hobbs, G. Kresse, J. Hafner, Phys. Rev. B 62 (2000) 11556.
[18] J. Tersoff, D.R. Hamann, Phys. Rev. B 31 (1985) 805.
[19] J.R. Osiecki, H.M. Sohail, P.E.J. Eriksson, R.I.G. Uhrberg, Phys. Rev. Lett. 109 (2012) 057601.
[20] J.A. Stroscio, D.M. Eigler, Science 254 (1991) 1319.
[21] P. Avouris, Acc. Chem. Res. 28 (1995) 95.
[22] A.A. Saranin, T. Numata, O. Kubo, H. Tani, M. Katayama, V.G. Lifshits, K. Oura, Phys. Rev. B 56 (1997) 7449.
[23] A.A. Saranin, A.V. Zotov, V.G. Kotlyar, I.A. Kuyanov, T.V. Kasyanova, A. Nishida, M. Kishida, Y. Murata, H. Okado, M. Katayama, K. Oura, Phys. Rev. B 71 (2005) 035312.
[24] A.A. Saranin, A.V. Zotov, V.G. Lifshits, J.-T. Ryu, O. Kubo, H. Tani, T. Harada, M. Katayama, K. Oura, Surf. Sci. 429 (1999) 127.
[25] I.M. McLeod, V.R. Dhanak, A. Matilainen, M. Lahti, K. Pussi, K.H.L. Zhang, Surf. Sci. 604 (2010) 1395.
[26] K. Yaji, Y. Ohtsubo, S. Hatta, H. Okuyama, K. Miyamoto, T. Okuda, A. Kimura, H. Namatame, V. Taniguchi, T. Aruga, Nat. Commun. 1 (2010) 17.
[27] A. Höpfner, J. Schäfer, A. Fleszar, J.H. Dil, B. Slomski, F. Meyer, C. Loho, C. Blumenstein, L. Patthey, W. Hanke, R. Claessen, Phys. Rev. Lett. 108 (2012) 186801.
[28] L.V. Bondarenko, D.V. Gruznev, A.A. Yakovlev, A.Y. Tupchaya, D. Usachov, O. Vilkov, A. Fedorov, D.V. Vyalikh, S.V. Eremeev, E.V. Chulkov, A.V. Zotov, A.A. Saranin, Sci. Rept. 3 (2013) 1826.